A Multidiscipline and Multi-rate Modeling Framework for Planar Solid-oxide-fuel-cell based Power-Conditioning System for Vehicular APU

Sudip K. Mazumder
Dept of Electrical & Computer Engineering
Lab for Energy and Switching-electronics Systems
University of Illinois at Chicago
mazumder@ece.uic.edu

Sanjaya K. Pradhan
Sanjaya.K.pradhan@Philips.com

Joseph Hartvigsen
SOFC & Hydrogen Technologies, Ceramatec
joe@h-hydro.com

Diego Rancruel
New Product Introduction, GE Power Generation Technology
rancruel@hotmail.com

Michael R. von Spakovsky
Department of Mechanical Engineering, Center for Energy Systems Research
Virginia Polytechnic Institute and State University
vonspako@vt.edu

Moe Khaleel
Computational Sciences & Mathematics Division, Pacific Northwest National Laboratory
moe.Khaleel@pnl.gov

A numerical modeling framework for planar solid-oxide fuel cell (PSOFC) based vehicular auxiliary power unit (APU) is developed. The power-conditioning system (PCS) model comprises the comprehensive transient models of PSOFC, balance-of-plant and power-electronics subsystems (BOPS and PES, respectively) and application load (AL). It can be used for resolving the interactions among PSOFC, BOPS, PES and AL, control design and system optimization and studying fuel-cell durability. The PCS model has several key properties including: (i) it can simultaneously predict spatial as well as temporal dynamics; (ii) it has two levels of abstraction: comprehensive (for detailed dynamics) and reduced-order (for fast simulation); and (iii) the fast-simulation model can be implemented completely in Simulink/Matlab environment, thereby significantly reducing the cost as well as time and provides the avenue for real-time simulation and integration with vehicular power-train models employing the widely used ADVISOR. The computational overhead and accuracy of the fast-simulation and comprehensive models are compared. Significant savings in time compared to using the former were obtained, without compromising accuracy.

Keywords: Modeling, planar solid-oxide fuel cell (SOFC), auxiliary power unit (APU), power electronics, power conditioning, balance of plant (BOP)

SIMULATION, Vol. 84, Issue 8/9, August/September 2008 413–426
© 2008 The Society for Modeling and Simulation International
DOI: 10.1177/0037549708097713
Figures 1, 2, 4–11 appear in color online: http://sim.sagepub.com

1. Introduction

Among several potential fuel cells considered for auxiliary-power units (APUs) [1–3], planar solid-oxide

fuel cells (PSOFCs) are emerging as one of the prime candidates primarily because of their high energy-conversion efficiency, power density and fuel flexibility [4]. Recently, modeling of the power-conditioning system (PCS) for a PSOFC based APU has gained importance [5]. Such a modeling framework potentially addresses key issues including resolving the interactions among PSOFC, balance-of-plant subsystem (BOPS), power-electronics subsystem (PES) and application load (AL), control design and system optimization, integration of the system model with actual vehicle-system model and enabling real-time simulation (RTS) for long-term durability studies.

A tubular SOFC (TSOFC) based temporal PCS modeling framework for a residential power system was demonstrated [6], as shown in Figure 1. This powerful multi-software modeling framework comprises models of BOPS (implemented in gPROMS [7]), TSOFC (implemented in Visual Fortran) and PES (implemented in Saber designer [8]) and an AL profile. Because each of the subsystem models is developed in proven platforms, it is relatively simple to design the overall PCS. However, this introduces the following limitations: (i) relatively expensive overall software platform; (ii) high computational overhead, due to: the need for data exchange via the iSIGHT software [9] interface; the high order of the overall comprehensive PCS model (e.g. order of the BOPS model greater than 450); and the significant variation in scales among the PES switching model and the BOPS and TSOFC models; (iv) no spatial data of the TSOFC is obtainable without freezing the time; and (v) the system modeling framework does not provide any avenue for RTS of the PCS.

To address the computational overhead and high simulation cost, a Simulink/Matlab based modeling framework comprising the models of BOPS, PSOFC-stack, and PES was developed [5] for vehicular APUs. This framework is relatively inexpensive and allows fast simulation. Because the BOPS and the PSOFC models are based on steady-state thermo-electro-chemical empirical models, the steady-state response of the system is reasonably accurate. However, the modeling framework has the following limitations: (i) since the PSOFC model is based on teady-state empirical data only, its transient predictions may not be accurate; (ii) the BOPS model is highly simplified and derived primarily from steady-state empirical data; (iii) the PES model being developed based on the power balance cannot predict any transient effect; and (iv) no spatial data of the PSOFC is obtainable. Thus, the model in its present form [5] cannot predict accurately the effect of the load transients and other electric-feedback effects on the PSOFC and the performance of the PSOFC based vehicular APU for control and system optimization.

To alleviate current limitations [5, 6], we develop a numerical modeling framework for a PSOFC APU. This framework can provide spatial (up to two dimensions) as well as temporal data simultaneously. It has the ability to work with comprehensive transient models of PSOFC, BOPS, PES and AL profile for vehicular APU if one needs to focus on details, or with reduced-order models for fast computation and RTS and integration with bigger vehicular-system model. Finally, because the system model is developed primarily in Simulink/Matlab environment, the software cost is minimal.

2. System-Modeling Framework

Figure 2a shows the new comprehensive modeling framework while Figure 2b shows the reduced-order modeling framework for faster simulation. The system models comprise PSOFC, BOPS, PES and AL profile. While the comprehensive model requires two low-cost software programs for implementation (Simulink/Matlab including SimPowerSystem and gPROMS including gO:Simulink), the reduced-order model requires only Simulink/Matlab including SimPowerSystem. As such, apart from being faster, the latter is also suitable for RTS using Mathwork's Real Time Workshop [10] and may also enable the integration of the model with vehicular power-train models using the widely used ADVISOR [11], as illustrated in Figure 2b.

2.1 PSOFC Model

2.1.1 Two-Dimensional PSOFC Model

For accurate prediction of the effects of system interactions on the PSOFC, one needs to analyze the PSOFC internal parametric variations [12–17]. Because a transient model of the PSOFC [6] cannot predict the spatial dynamics, we have developed a spatio-temporal electro-thermo-chemical model of the PSOFC (in Simulink), which provides spatial discretizations of the cell. This model is designed to accept required system inputs (reactant stream flow rates, compositions, and temperatures, cell geometric parameters, and cell current) and computes the corresponding spatial properties of the fuel cell.

The cell temperature T in the two-dimensional (x and y) model, as shown in Figure 3, is computed from the time-dependent solution of:

$$\rho C_p \frac{\partial T}{\partial t} - k\left(\frac{\partial T^2}{\partial x^2} + \frac{\partial T^2}{\partial y^2}\right) = Q \tag{1}$$

where

$$Q = \left(\frac{V_{\text{tn}} - V_{\text{op}}}{l}\right) ji + (-\Delta H_{\text{shift}}) \tag{2}$$

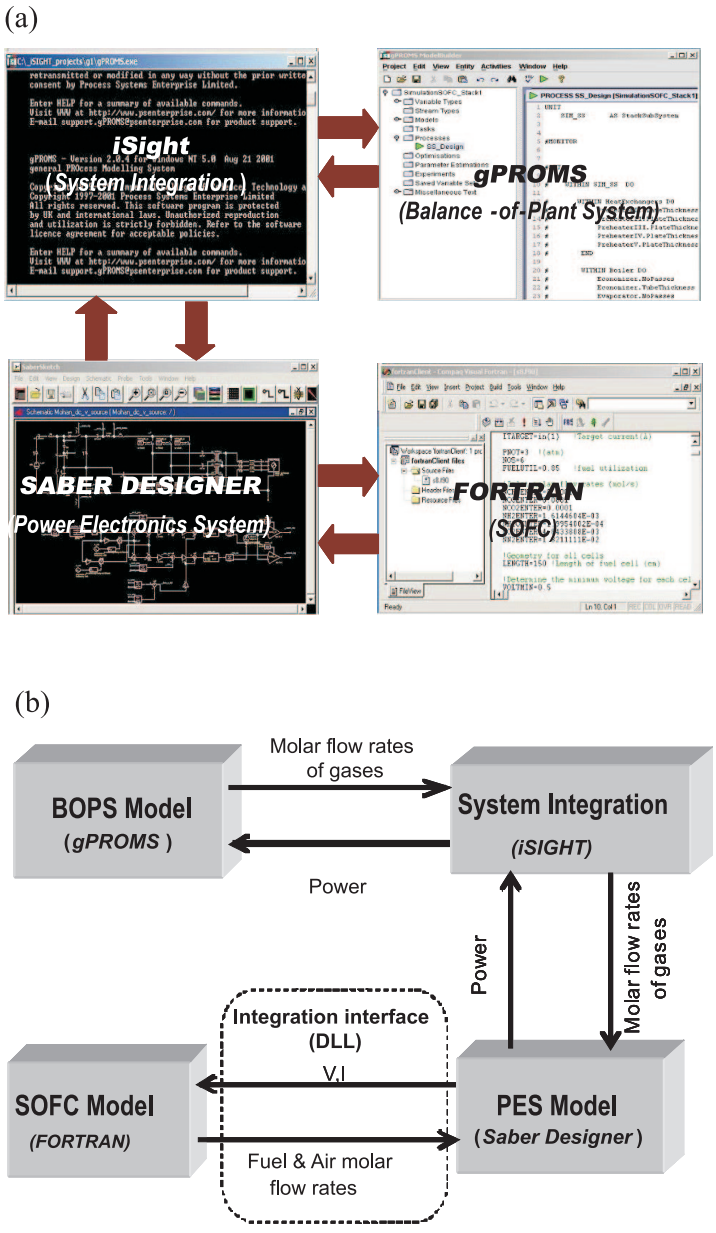

Figure 1. (a) A multi-software platform [5] for the simulation of a TSOFC PCS and (b) the flow of data among the different software packages. The arrows indicate the direction of data flow in the model.

and V_{tn} is the thermal neutral voltage, V_{op} is the operating voltage, ji is the current density, ρ is the mass density of the control volume, C_p is the combined specific heat at constant pressure, l is the cell thickness, ΔH_{shift} is the enthalpy of the shift reaction and k is the thermal conductivity of the fuel cell. To approximate the second-order partial-differential equation, we use a finite-difference method using central differences [18] and obtain

$$\frac{\partial T^2}{\partial x^2} \approx \frac{1}{\Delta x^2}\left[T_{m+1,n,t} - 2T_{m,n,t} + T_{m-1,n,t}\right] \quad (3a)$$

$$\frac{\partial T^2}{\partial y^2} \approx \frac{1}{\Delta y^2}\left[T_{m,n+1,t} - 2T_{m,n,t} + T_{m,n-1,t}\right]. \quad (3b)$$

By approximating $\partial T/\partial t$ as a simple forward difference and substituting $[(T_{j+1}-T_j)/\Delta t]$ for $\partial T/\partial t$, substituting Equation (2) into Equation (1), and marching the solution

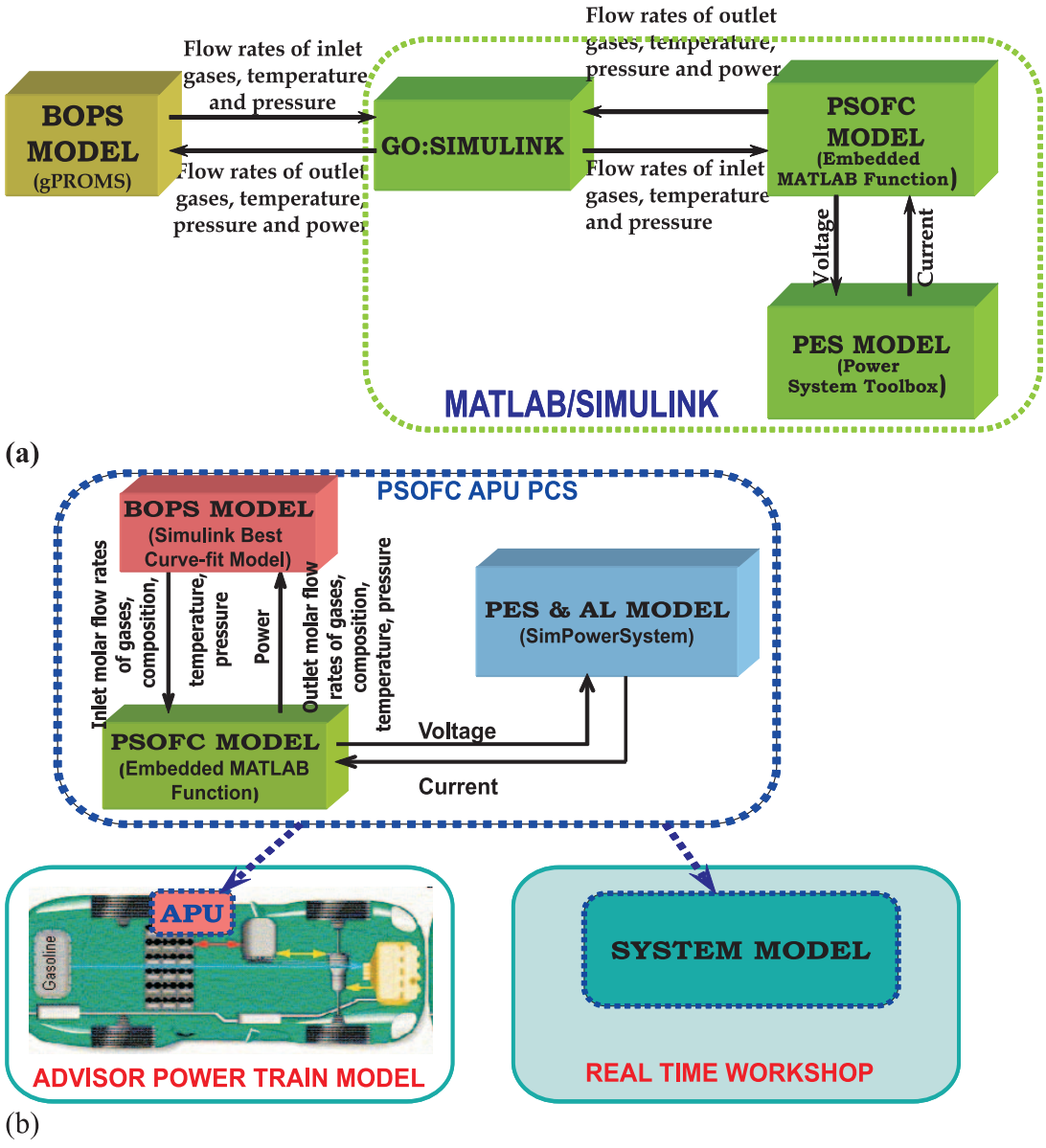

Figure 2. (a) **M**odeling framework for a comprehensive PSOFC-based PCS for a vehicular APU. (b) Reduced-order modeling framework for PSOFC-based PCS, developed in Simulink/Matlab platform, thereby enabling RTS and the possibility for integration with vehicular power-train model in ADVISOR.

through time (assuming step size $\Delta x = \Delta y$) yields the Euler's explicit-integration scheme:

$$T_{m,n,t+1} = T_{m,n,t} + \frac{k\Delta t}{\rho C_p \Delta x^2}(T_{m-1,n,t} + T_{m,n-1,t} + T_{m,n+1,t} + T_{m+1,n,t} - 4T_{m+1,n,t}) + \frac{\Delta t}{\rho C_p} Q. \quad (4)$$

The thermal neutral voltage and Nernst (En is the Nernst potential) potential for the PSOFC are defined as

$$V_{\text{tn}} = -\frac{\Delta H_{\text{shift}}}{nF} \quad (5)$$

$$En_{m,n} = -\frac{\Delta G}{nF} \quad (6)$$

where ΔG is the change in the Gibb's free energy and ΔH is the enthalpy of reaction, n is the number of electron

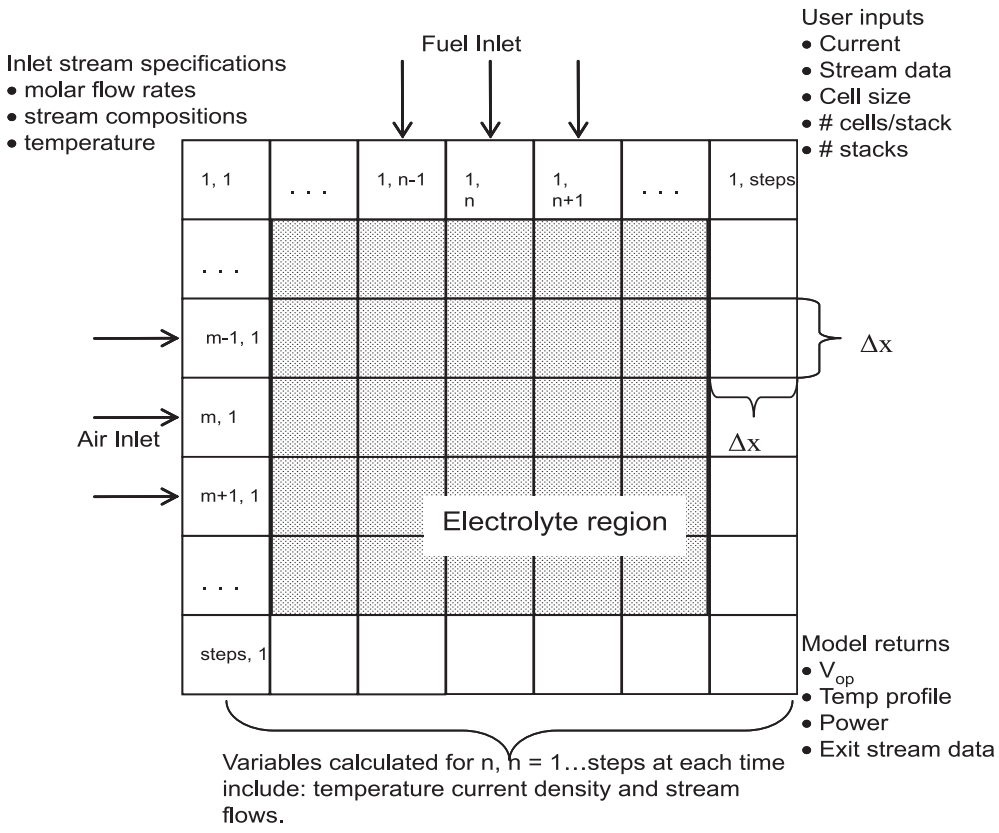

Figure 3. Spatial homogenous model for the PSOFC providing two-dimensional discretizations involving finite-difference method.

transfer per reaction. To accommodate the specification of current as an independent variable, with cell operating voltage as the computed dependent variable, the initial value of the operating voltage (used to compute the heat generation term in Equation (2)) is approximated by

$$V_{\text{op}} = En_{m,n} - ji.\text{ASR}_{m,n} \tag{7}$$

where $\text{ASR}_{m,n}$ is the local temperature-dependent area-specific resistance. In the course of each of the iterations, the assumed operating voltage is used to determine the current density in each of the control volumes throughout the cell using

$$ji_{m,n} = \frac{(En_{m,n} - V_{\text{op}})}{\text{ASR}_{m,n}} \tag{8}$$

which is then summed as shown in Equation (9) to compute the total cell current:

$$I = \sum_{m=1}^{\text{steps}} \sum_{n=1}^{\text{steps}} \left(\Delta x \Delta y \frac{En_{m,n} - V_{\text{op}}}{\text{ASR}_{m,n}} \right). \tag{9}$$

These local current-flux values are used to determine the change in stream composition based on the reaction in each control volume:

$$H_2 + \frac{1}{2}O_2 \rightarrow H_2O. \tag{10}$$

The fuel exit-composition of each control volume is equilibrated with respect to the shift reaction before entering the downstream control volume. Equation (11) is used to adjust the compositions to enforce the shift equilibrium constraint at the entrance to each control volume:

$$K_p = e^{-\Delta G_o/\text{RT}} = \frac{(p_{CO_2} + \omega)(p_{H_2} + \omega)}{(p_{CO} - \omega)(p_{H_2O} - \omega)} \tag{11}$$

where ΔG_o is a temperature-dependent variable [19], p_{CO_2}, p_{H_2}, p_{CO}, and p_{H_2O} are the partial pressures of CO_2, H_2, CO and H_2O, respectively, K_p is the constant of equilibrium, R is the universal gas constant and ω is the adjustment in the gas compositions due to the shift reaction.

2.1.2 One-dimensional PSOFC Model

Using the homogeneous slab model for the PSOFC (shown in Figure 4), the one-dimensional spatio-temporal model of the PSOFC is derived from its two-dimensional form (i.e. Equations (1–11)) by discretizing only in one dimension (x). The equation summary of the one-dimensional PSOFC model is tabulated in Table 1.

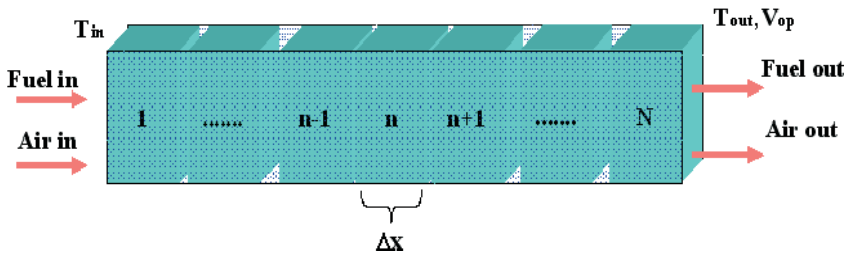

Figure 4. One-dimensional homogenous slab model for PSOFC providing discretizations involving finite-difference method. Temperature, current and molar-flow rates of air and fuel are calculated each time for $n = 1,\ldots,N$.

Table 1. Summary of the derivation of the 1D model from the 2D model

$\rho C_p \frac{\partial T}{\partial t} - k\frac{\partial T^2}{\partial x^2} = Q$	$Q = \left(\frac{V_{\text{tn}} - V_{\text{op}}}{l}\right) ji_n + (-\Delta H_{\text{shift}})$
$\frac{\partial T^2}{\partial x^2} \approx \frac{1}{\Delta x^2}\left[T_{n+1,t} - 2T_{n,t} + T_{n-1,t}\right]$	$T_{n,t+1} = T_{n,\,t} + \frac{k\Delta t}{\rho C_p \Delta x^2}(T_{n+1,\,t} - 2T_{n,\,t} + T_{n-1,\,t}) + \frac{\Delta t}{\rho C_p} Q$
$V_{\text{tn}} = -\frac{\Delta H}{nF}$	$En_n = -\frac{\Delta G}{nF}$
$V_{\text{op}} = En_n - ji \times \text{ASR}_n$	$I = \sum_{n=1}^{\text{steps}} \left(\frac{\Delta x^2 (En_n - V_{\text{op}})}{\text{ASR}_n}\right)$
$ji_n = \frac{En_n - V_{\text{op}}}{\text{ASR}_n}$	$K_p = e^{-\Delta G_o/\text{RT}} = \frac{(p_{\text{CO}_2} + \omega)(p_{\text{H}_2} + \omega)}{(p_{\text{CO}} - \omega)(p_{\text{H}_2\text{O}} - \omega)}$

2.2 PES Modeling

2.2.1 Switching Model for Global Dynamics

The PES topological model for the APU is shown in Figure 5. The model essentially consists of a DC-DC buck-derived converter to step-down the PSOFC output voltage to an intermediate DC bus voltage (42 V). An inverter is used to convert the DC bus voltage to feed the AC power bus. Further, the intermediate DC bus voltage is stepped down using a bidirectional buck/boost derived converter to supply the 12 V DC loads and to charge the battery. The rated voltage of the PSOFC stack is between 72–90 V. As such, the front-end 42 V DC-DC converter for the 5 kW APU has to be unidirectional (because current should not flow into the fuel cell) and a step-down converter, which regulates the output voltage at 42 V. A full-bridge converter, as shown in Figure 5, is chosen to meet the requirements. The operational details of the converter are outlined in [20]. The switches S1 and S3 and S2 and S4 switch in complementary pairs, with a time delay between the switching of S1 (S3) and S2 (S4). This phase delay between the switching signals of S1 (S3) and S2 (S4) is controlled to obtain the desired output voltage.

The DC-AC inverter provides power to the AC loads at 115 V (rms). First, the isolated DC-DC Ćuk converter, as shown in Figure 5, boosts the input voltage to a high intermediate DC voltage and subsequently the voltage-source inverter (VSI) steps the high-voltage DC to 115 V AC (rms). For operation details of the Ćuk converter and the VSI see [21, 22]. Briefly, a sinusoidally-modulated switching sequence is generated for SW1 (SW3) and SW2 (SW4) to obtain an averaged sine wave at the output of the VSI. The only switching constraint is that SW1 (SW2) and SW3 (SW4) must operate in a complementary fashion. The operation of the Ćuk converter comprises two modes. In the first mode, SW5 and SW6 turn on (and the diodes on the secondary side turn off), thereby building the flux of the input and the output inductors. In the subsequent mode, SW5 and SW6 turn off (and the diodes on the secondary turn on), thereby the input and the output inductors build the electrostatic energy of the intermediate capacitors.

A full-bridge isolated bidirectional topology for the 12 V DC-DC converter is chosen, as shown in Figure 5. A flyback inductor is used in the low voltage (12 V DC) side to help the building of the voltage during startup in the boost mode. The operational details of the converter are outlined in [23]. This converter works in two modes decided by an external signal triggered by the level of the DC bus voltage. Whenever the 42 V bus sags, the 12 V converter works in a boost mode; on the other hand, when the bus voltage recovers, the converter operates in normal buck mode. A time-delay control for the bridge in the high-voltage side (for buck mode of operation) is used, which is similar to the control as described for the 42 V DC-DC converter above. In the boost mode, a current-mode control is implemented, in which two PWM sig-

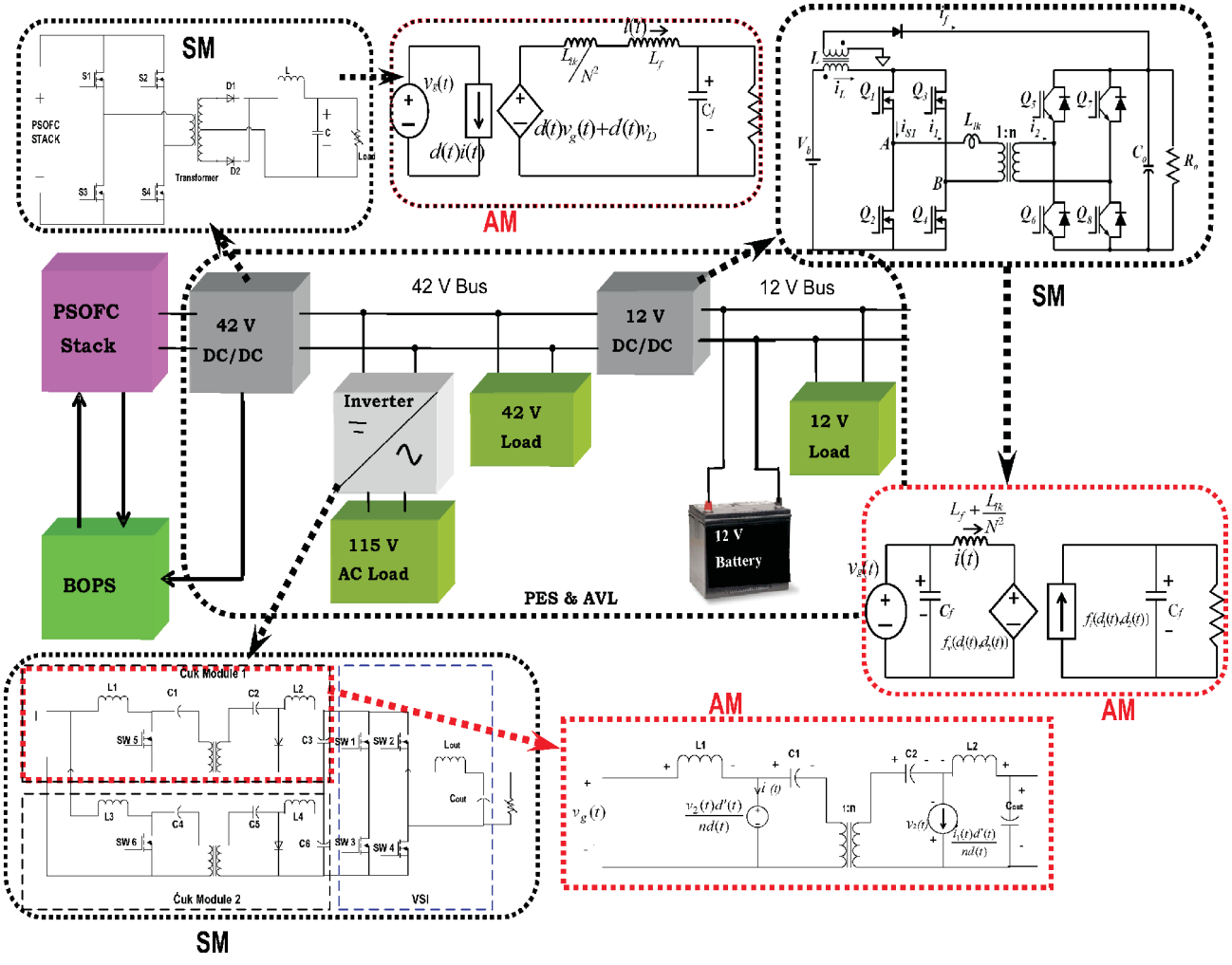

Figure 5. An architecture of the PES and the switching and corresponding averaged models (i.e. SM and AM, respectively) for the power converters. For all of the AMs, *d* represents the duty ratio.

nals which are 180° out of phase are used to generate the switching signals for Q1 (and Q4) and Q2 (and Q3), respectively.

2.2.2 Averaged Model for Fast Computation

Because the PES switching model comprises discontinuous-differential equations, a stiff solver and fast sampling is required for convergence and numerical stability. For example, to solve the switching model of a PES converter operating at 20 kHz (i.e. a switching period of 50 μsec), sampling time as low as hundreds of nanoseconds may be required. Comparing that to the vastly different (typical) sampling times of PSOFC and BOPS models (which are around a few milliseconds and hundreds of milliseconds, respectively), we realize that the PES switching model is one of the key hindrances to the fast computation of PSOFC PCS model.

Obviously, to increase the speed of the PCS simulation we need to avoid discontinuity, thereby reducing the sampling rate and bring it as close as possible to that required by the PSOFC and BOPS models without significantly compromising the accuracy. In one such approach [5], the PES is designed as a power converter with a constant-efficiency module, where output of the converter is a fixed fraction of the input power. However, this model is inaccurate as it assumes that the efficiency of the PES is constant for all load conditions. Further, and more importantly, this model does not predict the transient response of the PES.

An alternate approach to avoid discontinuity of the PES model is to use a map [24]. In a map, instead of solving the switching differential as a whole, we solve the overall models in finite time intervals by treating the PES as

a piecewise-linear system (PLS). Subsequently, using the commutative property, we piece together the solutions in each of intervals to construct the final solution in terms of the initial conditions of the states of the PES model. Although a map is a powerful and accurate approach, it typically requires the knowledge of the analytical solution of the PLS and the complexity of the solution increases with the order of the PES model.

As such, we adopted an averaged-modeling technique [25, 26] to analyze the behavior of the PES without significant computational overhead. Figure 5 shows the averaged models of the PES converters in equivalent-circuit form [26]. Notice that unlike the switching models (SMs), the averaged models (AMs) do not have any discontinuous elements. Further, the averaged (circuit) models enable the usage of built-in circuit modules in Simulink. It is noted that an averaged model ideally provides the averaged dynamics of the PES and as such it transforms the PES model from a discontinuous to a smooth form. The accuracy of the averaged model typically varies with the switching frequency, with higher accuracy for higher operating frequency.

2.3 BOPS Modeling

2.3.1 Overview of the Comprehensive Model

Figure 6 shows the initial BOPS configuration, which after a comprehensive synthesis/design and operational/control optimization changes fairly significantly [27]. The comprehensive details of the initial configuration are provided in [6]. Briefly, the BOPS model comprises a set of first-principle and semi-empirical equations for component and subsystem mass and energy conservation, kinetic behavior and geometry for both design and off-design operations. A sampling of some of these equations for a number of principal BOPS components are outlined below.

2.3.2 Modeling of the Steam Methane Reformer

A single adiabatic reactor tube is analyzed, where the dynamic mass balance on the reformate gas side is given by

$$\frac{\partial\left(-UC\right)}{\partial x}-R_{\mathrm{a}}\rho_{\mathrm{C}}=\frac{\partial C}{\partial t} \tag{12}$$

where C is the methane molar concentration (g-mole m^{-3}), U is the superficial velocity, R_a is the methane reaction rate per unit mass of catalyst, ρ_{C} is the catalyst bed density and x is the axial direction.

The reformate gas-side energy balance is:

$$-\frac{\partial\left(FC_pT\right)}{\partial x}+\sum F\left(-\Delta H\right)\frac{\partial X}{\partial x}+h_{\mathrm{i}}A_{\mathrm{i}}\left(T_{\mathrm{w}}-T\right)$$

$$+\ h_{\mathrm{c}}A_{\mathrm{c}}A_{\mathrm{i}}\left(T_{\mathrm{c}}-T\right)=A_{\mathrm{i}}C_p\frac{\partial\left(\rho T\right)}{\partial t} \tag{13}$$

where

$$\sum F\left(-\Delta H\right)\frac{\partial X}{\partial x}\ =\ F_1\left(-\Delta H_1\right)\frac{\partial X_1}{\partial x}$$

$$+\ \left(F_3+X_1F_1\right)\left(-\Delta H_2\right)\frac{\partial X_2}{\partial x} \tag{14}$$

where C_p is the heat capacity of the tube-side, A_c is the external surface area of particles per volume of catalyst bed, T_c is the catalyst temperature, h_i is the inside heat transfer coefficient, h_c is the catalyst-fluid heat transfer coefficient, ΔH_1 is the demethanation reaction enthalpy and ΔH_2 is the water-gas shift reaction enthalpy. In Equation (14), X_1 and X_2 represent the conversions of the demethanation and water-gas shift reactions, respectively. After spatial discretization, the reaction enthalpies are evaluated at each reactor segment's average temperature.

2.3.3 Modeling of the Compact Heat Exchangers

The energy analysis of each discretized section of the heat exchanger for hot and cold sides and wall is given by

$$\left(MC_p\right)_{\mathrm{H}}\frac{\partial T_{\mathrm{H}}}{\partial t}\ =\ \left(\dot{m}C_p\right)_h L_x\frac{\partial T_{\mathrm{H}}}{\partial x}$$

$$+\ \left(hA\right)_{\mathrm{H}}\left(T_{\mathrm{H}}-T_{\mathrm{W}}\right) \tag{15}$$

$$\left(MC_p\right)_{\mathrm{C}}\frac{\partial T_{\mathrm{C}}}{\partial t}\ =\ \left(\dot{m}C_p\right)_{\mathrm{C}}L_y\frac{\partial T_{\mathrm{C}}}{\partial y}$$

$$+\ \left(hA\right)_{\mathrm{C}}\left(T_{\mathrm{C}}-T_{\mathrm{W}}\right) \tag{16}$$

$$\left(MC_p\right)_{\mathrm{W}}\frac{\partial T_{\mathrm{W}}}{\partial t}\ =\ \left(hA\right)_{\mathrm{C}}\left(\bar{T}_{\mathrm{C}}-T_{\mathrm{W}}\right)$$

$$+\ \left(hA\right)_{\mathrm{H}}\left(\bar{T}_{\mathrm{H}}-T_{\mathrm{W}}\right) \tag{17}$$

where M is the mass in the control volume, subscripts C and H indicate the cold and hot sides, subscript W the wall, x and y are the longitudinal and transverse directions, respectively, A refers to the heat transfer area and h refers to the heat transfer coefficients.

2.3.4 Modeling of the Methane and Air Compressors

In the compressor, heat flows from the fluid to the casing to the ambient as well as from the fluid to the impeller to the casing and to the ambient through the bearings, seals and shaft. The thermal capacitance of the casing, impeller and inlet duct can be approximated by a single thermal mode at a temperature T_{o} such that

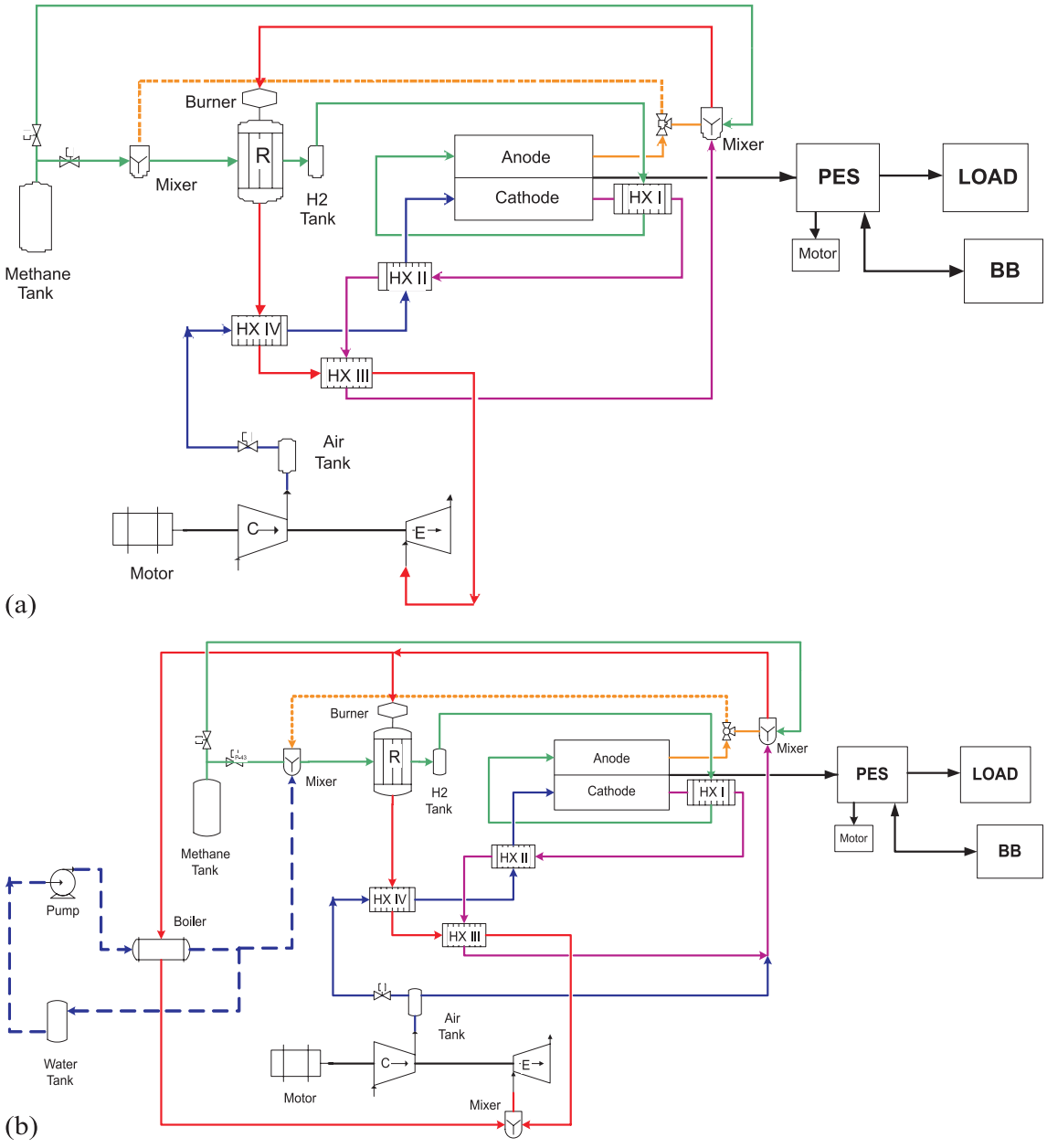

Figure 6. (a) Optimum configuration resulting from the Phase I/Phase II reduced super-configuration during synthesis/design and operation/control optimization. (b) Optimum start-up configuration resulting from the dynamic synthesis/design and operation/control optimization process.

$$mC_p \frac{\partial T_o}{\partial t} = (hA)_i \left[\frac{T_1 + T_2}{2} - T_o \right] - (hA)_o (T_o - T_{amb}) \quad (18)$$

where m is the mass of the thermal mode, C_p is the thermal mode specific heat, $(hA)_i$ is the inner conductance from the fluid to the thermal mode, $(hA)_o$ is the outer conductance from the thermal mode to the ambient, T_o is the thermal mode temperature and T_{amb} is the ambient temperature.

The shaft component is used to compute the turbomachinery rotational speed N based on input values of turbine power output and compressor power input. A power balance yields

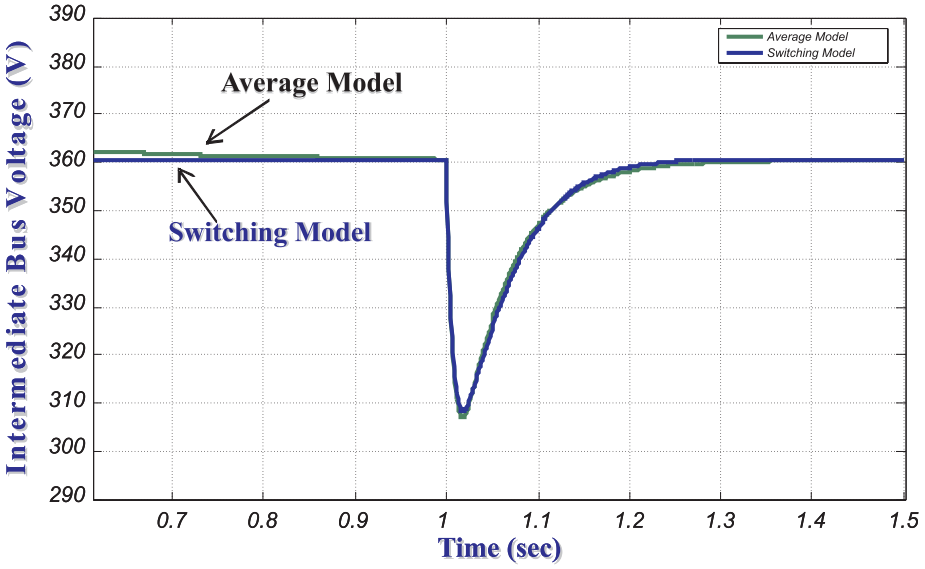

Figure 7. Accuracy of the PES averaged model, illustrated by comparing the averaged dynamics of the DC-DC isolated Ćuk converter (when subjected to a load transient at t = 1 s) with its switching dynamics.

$$IN\frac{\partial N}{\partial t} = \Delta W \tag{19}$$

where I is the moment of inertia and ΔW is the power balance on the component. The transient heat transfer model for an expander is similar to that for compressors and scalable performance maps are used for both types of components to simulate off-design behavior.

2.3.5 Polynomial-Approximation Model

The very high order of the BOPS model (about 450) significantly increases the computational overhead of the system simulation. An added reason for higher computation time is the need for interfacing between the gPROMS and Simulink/Matlab models via the gO:Simulink interface. As such, the prime need is to reduce the order of the BOPS model and implement the approximate model in the Simulink/Matlab platform to reduce computational time and enable RTS. To realize the polynomial-approximation model, we first subjected the BOPS model to different sets of load transients and steady-state electrical feedbacks. The transient responses of all the output BOPS parameters (such as temperature, air and fuel flow rates and air and fuel compositions), which are used to interface the BOPS model to the PSOFC model, are stored in a database. Subsequently, we applied multi-order (starting from linear to seventh-order) polynomial approximations on each set of these data to obtain the closest approximation that provides optimal compromise between speed of simulation and accuracy with regard to the data obtained using the comprehensive model. A similar approach is adopted to reduce the order of the BOPS model in [5].

3. Results

Table 2 shows the percentage improvement in simulation time obtained using the reduced-order models of the PSOFC, PES and BOPS. The simulation time is based on 10 s of individual subsystems of the PSOFC PCS simulation on a two-processor Intel Xeon PC, with each processor operating at 2 GHz. A significant improvement is obtained using the PES averaged model because the averaged model transforms the problem from analyzing a discontinuous-nonlinear differential equation (where an accurate determination of the switching transients is necessary, leading to high computational overhead) to analyzing a smooth differential equation. Importantly, since the switching frequencies of the converters are high, the dynamics of the PES obtained using the average models are close to that obtained using the corresponding switching model. The polynomial approximation of the comprehensive BOPS model yields significant savings in time without compromising accuracy. This is also true for the PSOFC one-dimensional model.

Figures 7–9 illustrate the accuracy of the results obtained using fast-computational models (comprising polynomial-approximation model of the BOPS, averaged model of the PES, and the one-dimensional PSOFC model). Figure 7 depicts the comparison between the averaged and the switching model of the PES, using the isolated DC-DC Ćuk converter (shown in Figure 5) as an illustration. The Cuk converter is initially in steady state and is then subjected to a load transient at t = 1 s. For the same load transient, Figure 8 shows the comparison of the corresponding responses between the two- and

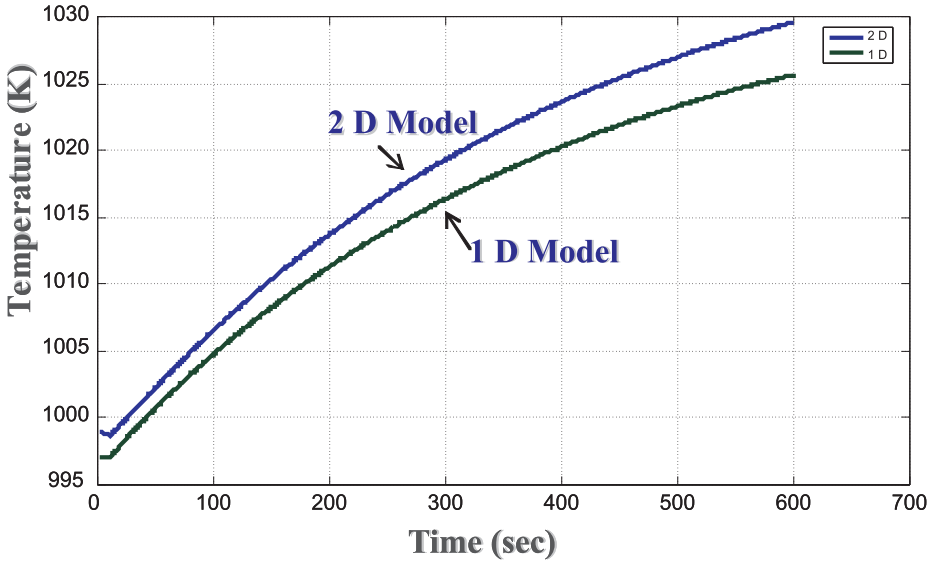

Figure 8. Comparison of the mean cell temperature of the PSOFC (when subjected to the load transient at t = 1 s) obtained using its one- and two-dimensional models.

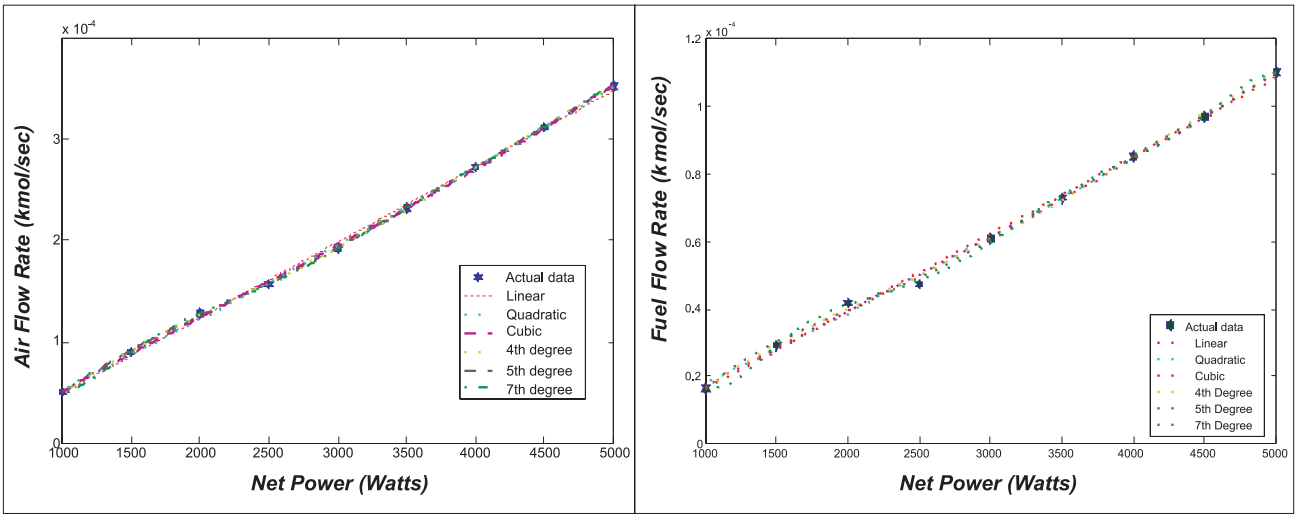

Figure 9. Polynomial approximation of the air- and fuel-flow rates of the BOPS model versus net power.

one-dimensional PSOFC model. Clearly, there is a close match between the responses of the reduced-order and comprehensive PES and PSOFC models. The polynomial approximation of the BOPS response is illustrated in Figure 9. A fifth-order polynomial approximation was chosen to achieve the optimal compromise between simulation speed and accuracy.

Figures 10 and 11 illustrate the responses of the PSOFC PCS model, obtained using the reduced-order/approximate models of the PSOFC, PES and BOPS. The PCS is subjected to a load transient at t = 1 s as shown in Figure 10a. The corresponding variations in the PSOFC fuel utilization and output voltage are shown in Figure 10b. An increase in the fuel utilization leads to an increase in the cell temperature. However, the temperature change is not appreciable at t = 1 s. This is because although the fuel utilization changes immediately due to the low electro-chemical time constant of the PSOFC, the change in the cell temperature is not immediate due to the higher thermal time constant of the cell. As such, and as

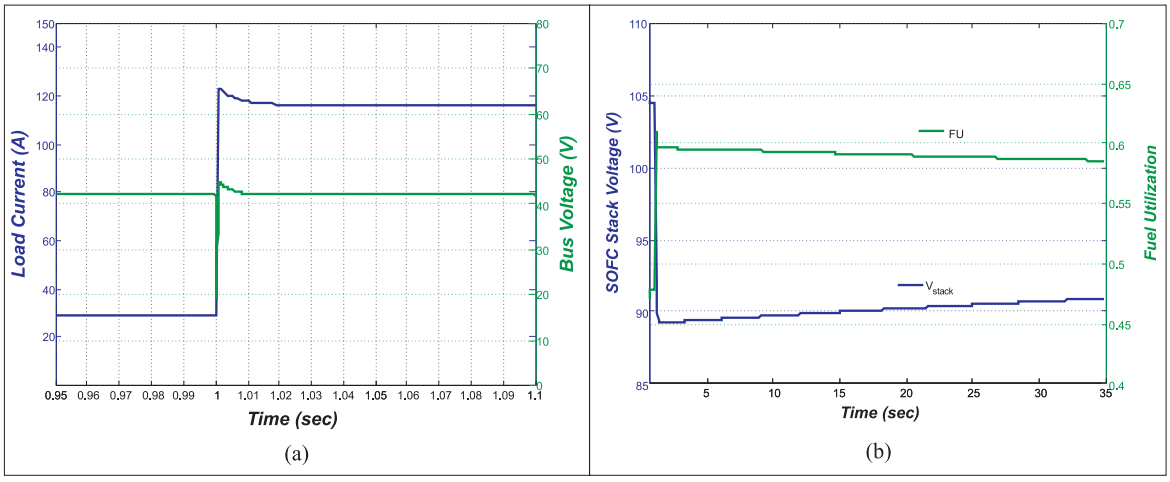

Figure 10. (a) Bus voltage and load current during and after the load-transient. (b) Variation of the PSOFC stack voltage and its fuel utilization when it is subjected to a load transient at t = 1 s.

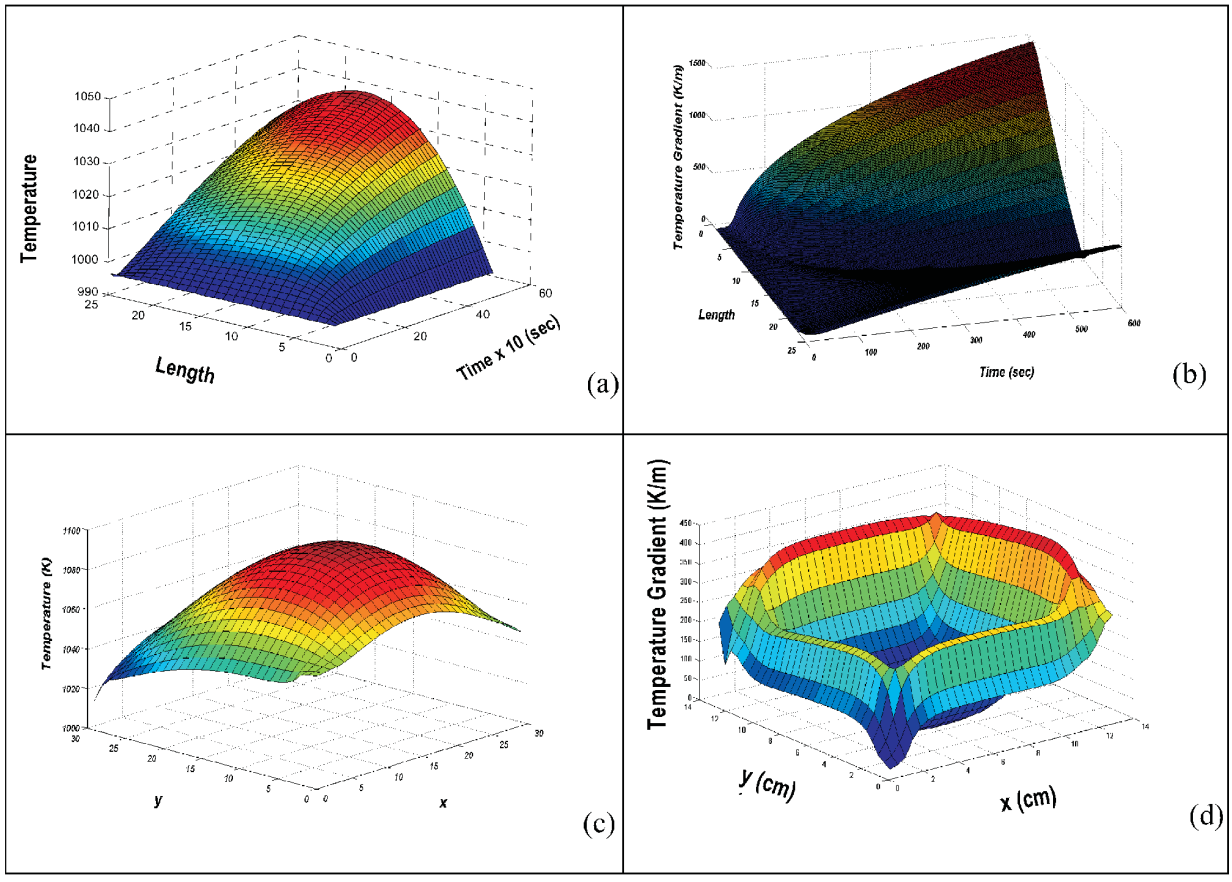

Figure 11. (a,b) Temperature and temperature-gradient distributions from t = 1 s to t = 600 s obtained using the one-dimensional PSOFC model. (c) Spatial-temperature distribution at t = 1 s and t = 600 s using the two-dimensional PSOFC model. (d) Temperature-gradient distribution obtained using the two-dimensional model of the system at t = 600 s.

Table 2. Reduction in computational overheads and comparison of accuracies (simulation time % is the ratio of the fast computational model time to the comprehensive model time)

Subsystems	Models being compared	Simulation time (%)	Computational error (%)
PES	Averaged model, switching model	0.945	1.12
BOPS	7th-order polynomial fit, comprehensive model	37.87	2.89
	5th-order polynomial fit, comprehensive model	27.45	3.29
	3rd-order polynomial fit, comprehensive model	21.7	9.40
	Linear fit, comprehensive model	16.17	13
PSOFC	One-dimensional, two-dimensional model	42.85	5.21

shown in Figure 11a, the change in the cell temperature, immediately after the load transient, is minimal. However, around 600 s after the transient, the net change in temperature reaches its peak. A more detailed picture of the cell temperature and gradient distributions (which provides a better insight into the cell stress) at that instant is shown in Figures 11c and 11d, which are obtained using the two-dimensional PSOFC model.

4. Conclusion

A low cost, numerical spatio-temporal modeling framework for simulating the dynamics of planar solid-oxide fuel cell (PSOFC) based power-conditioning system (PCS) for a vehicular auxiliary power unit (APU) is described. The PCS model, which comprises subsystem models of balance of plant, power electronics and PSOFC and the application-load profile, has two levels of abstraction: a high-order comprehensive model and a reduced-order fast-simulation model. The reduced-order model is obtained by a threefold effort. First, the power-electronics system model is transformed from a switching model to an averaged model, thereby significantly reducing the need for fast sampling to handle discontinuity. Second, a polynomial-approximation model is used for the high-order BOPS model. Third, an one-dimensional (instead of two-dimensional) spatio-temporal PSOFC model is used to reduce computational overhead.

As seen from Table 2, the fast-simulation model saves time without compromising accuracy. Overall, the newly-developed system model can be used for resolving system interactions and optimizations and control design in a low-cost framework. Further, because the fast-simulation model is implemented completely in Simulink/Matlab environment, it can be used for fuel-cell durability studies and real-time simulation (e.g. using Mathwork's Real Time Workshop) and potentially for integration with vehicular power-train models employing the widely-used ADVISOR.

5. Acknowledgements

This paper is prepared with the support of the US Environmental Protection Agency (Award No. RD-83158101-0), Pacific Northwest National Laboratory (Award No. 494828), Department of Energy (Award No. DE-FC2602NT41574), National Science Foundation CAREER (Award No. 0239131) and Office of Naval Research Young Investigator (Award No. N000140510594) received by Prof. Mazumder. However, any opinions, findings, conclusions or recommendations expressed herein are those of the authors and do not necessarily reflect the views of these supporting organizations.

6. References

[1] Brodrick, C.J., M. Farshchi, H.A. Dwyer, S.W. Gouse, M. Mayenburg, and J. Martin. 2000. Demonstration of a proton exchange membrane fuel cell as an auxiliary power source for heavy trucks. *Society of Automotive Engineers*, Paper 2000-01-3488. International Truck and Bus Meeting and Exposition, December 2000, Portland, OR, USA.

[2] Zizelman, J., S. Shaffer, and S. Mukerjee. 2002. Solid oxide fuel cell auxiliary power unit – a development update. *Society of Automotive Engineers*, paper 2002-01-0411. SAE 2002 World Congress and Exhibition, March 2002, Detroit, MI, USA.

[3] Grupp, D., M. Forrest, P. Mader, C.J. Brodrick, M. Miller, and H. Dwyer. 2004. *Design considerations for a PEM fuel cell powered truck APU*. Institute of Transportation Studies, UC Davis, UCD-ITS-RR-04-16, 2004.

[4] Lasher, S., Gouse, B., and C.J. Broderick. 2003. Assessment of fuel cells as auxiliary power systems for transportation vehicles. *Hydrogen and Fuel cells Merit Review Meeting*, Berkeley, CA. (Available at: http://www.tiax.biz/industries/pdfs/fuelcells/fc-apus_0114-03.pdf)

[5] Khaleel, M., B. Koeppel, and S. Moorehead. 2004. Modeling and control of a solid oxide fuel cell auxiliary power unit. *2004 DOE Hydrogen, Fuel Cells & Infrastructure Technologies*. (Available at http://www.eere.energy.gov/hydrogenandfuelcells/pdfs/review04/fc_48_khaleel_04.pdf)

[6] Mazumder, S.K., K. Acharya, C.L. Haynes, R. Williams, M.R. von Spakovsky, D.J. Nelson, D.F. Rancruel, J. Hartvigsen, and R.S. Gemmen. 2004. Solid-oxide-fuel-cell performance and durability: resolution of the effects of power-conditioning systems and application load. *Special Issue on Distributed Generation, IEEE Transactions of Power Electronics* 19: 1263–1278.

[7] http://www.psenterprise.com/products_gproms.html

[8] http://www.synopsys.com/cgi-bin/ces/detail.cgi?id=1200

[9] http://www.engineous.com/index.htm

[10] http://www.mathworks.com/access/helpdesk/help/toolbox/rtw/rtw_ug/f19735.html.

[11] http://www.ctts.nrel.gov/analysis/hev_test/modeling.shtml.

[12] Ferguson, J.R., J.M. Fiard, and R. Herbin. 1996. A mathematical model of solid oxide fuel cells. *Journal of Power Sources* 58: 109–122.

[13] Hartvigsen, J., S. Elangovan, and A. Khandkar. 1993. *Science and Technology of Zirconia V*. Edited by Badwal, S., Bannister, M., and Hannink, R., Technomic Publishing Company, Inc., Lancaster, Pennsylvania.

[14] Yentekakis, I.V., S. Neophytides, S. Seimanides, and C.G. Vayenas. 1993. Mathematical modeling of cross-flow, counter-flow and cocurrent-flow solid oxide fuel cells: theory and some preliminary experiments. *Proceedings of 2nd International Symposium on Solid Oxide Fuel Cells,* Athens, Greece, Official. Publication of the EEC, Luxembourg, pp. 281–288.

[15] Erdle, E., J. Gross, H.G. Muller, W.J.C. Müller, H.-J. Reusch, and R. Sonnenschein. 1991. *Modelling of Planar SOFC stacks*, Proceedings of the Second International Symposium on SOFCs, The European Commission, Brussels, pp. 265.

[16] Ferguson, J.R. 1991. *Analysis of temperature and current distribution in planar SOFC designs*, Proceedings of Second International Symposium on SOFCs, The European Commission, Brussels, pp. 305–312.

[17] Hendrikson, P.V. 1994. *Geilo*, Second Nordic Symposium on High Temperature Fuel Cells, Norway, March 16–18, 1994.

[18] Constantinides A. and N. Mostoufi. 1999. *Numerical Methods for Chemical Engineers with Matlab Applications*. Prentice Hall PTR. Upper Saddle River, New Jersey, USA.

[19] Barin, I. 1993. *Thermochemical Data of Pure Substances*, Edition 2. John Wiley & Sons Ltd., New York, USA.

[20] Redl, R., N.O. Sokal, and L. Balogh. 1990. A novel soft-switching full-bridge dc/dc converter; analysis, design considerations, and experimental results at 1.5kW, 100kHz. *IEEE Applied Power Electronics Conference*, pp. 162–172.

[21] Middlebrook, R.D. and S. Cuk. 1983. *Advances in Switched-Mode Power Conversion*, vols. I and II. TESLACO, CA.

[22] Mohan, N., T.M. Undeland, and W.P. Robbins. 1995. *Power electronics: converters, applications and design.* John Wiley & Sons, Singapore.

[23] Wang, K., F.C. Lee, and J. Lai. 2000. Bi-directional full-bridge dc/dc converter with unified soft-switching scheme, part I: principles of operation. *IEEE Applied Power Electronics Conference,* pp. 111–118.

[24] Mazumder, S.K., A.H. Nayfeh, and D. Boroyevich. 2001. Theoretical and experimental investigation of the fast- and slow-scale instabilities of a dc-dc converter. *IEEE Transactions on Power Electronics* 16(2): 201–216.

[25] Middlebrook, R.D. and S. Cuk. 1977. A general unified approach to modeling switching-converter power stages. *IEEE Power Electronics Specialists Conference*, pp. 521–550.

[26] Lee, F.C. 1990. *Modeling, Analysis, and Design of PWM Converter*, Virginia Power Electronic Center Publications Series, Blacksburg, Virginia.

[27] Rancruel, D. 2005. *Dynamic Synthesis/Design and Operation/Control Optimization Approach Applied to a Solid Oxide Fuel Cell based Auxiliary Power Unit under Transient Conditions*. Ph.D. thesis, Virginia Polytechnic Institute and State University, Blacksburg, VA.